Systematic aging of commercial LiFePO$_4$|Graphite cylindrical cells including a theory explaining rise of capacity during aging

Meinert Lewerenz [a, b, *], Jens Münnix [a, b], Johannes Schmalstieg [a, b], Stefan Käbitz [c], Marcus Knips [a, b], Dirk Uwe Sauer [a, b, c]

[a] Electrochemical Energy Conversion and Storage Systems Group, Institute for Power Electronics and Electrical Drives (ISEA), RWTH Aachen University, Jägerstrasse 17/19, D-52066, Aachen, Germany
[b] Juelich Aachen Research Alliance, JARA-Energy, Germany
[c] Helmholtz Institute Münster (HI MS), IEK-12, Forschungszentrum Jülich, Corrensstrasse 46, 48149, Münster, Germany

HIGHLIGHTS

- Passive electrode effect explains reversible capacity increase or decrease.
- Passive electrode effect includes influence of excess anode.
- Shallow cycling between 45 and 55% SOC results in highest aging.
- 4C tests result in less aging than lower C-rates.
- Thick covering layer are strongly influencing the cyclic aging.

ARTICLE INFO

ABSTRACT

The contribution introduces a new theory explaining the capacity increase that is often observed in early stages of life of lithium-ion batteries. This reversible and SOC-depending capacity rise is explained by the *passive electrode effect* in this work. The theory assumes a slow, compensating flow of active lithium between the passive and the active part of the anode, where the passive part represents the geometric excess anode with respect to the cathode. The theory is validated using a systematic test of 50 cylindrical 8 Ah LiFePO$_4$|Graphite battery cells analyzed during cyclic and calendaric aging. The cyclic aging has been performed symmetrically at 40 °C cell temperature, varying current rates and DODs. The calendar aging is executed at three temperatures and up to four SOCs. The aging is dominated by capacity fade while the increase of internal resistance is hardly influenced. Surprisingly shallow cycling between 45 and 55% SOC shows stronger aging than aging at higher DOD and tests at 4 C exhibit less aging than aging at lower C-rates. Aging mechanisms at 60 °C seem to deviate from those at 40 °C or lower.

The data of this aging matrix is used for further destructive and non-destructive characterization in future contributions.

© 2017 Elsevier B.V. All rights reserved.

1. Introduction

Lithium-ion batteries become more and more important and are replacing established battery types like lead-acid and NiMH batteries whenever high power density and space constraints are of major concerns. Even in terms of costs they become more competitive. The driving forces to develop this technology are consumer electronics, e-mobility and stability of the electrical grid with high penetration of renewable energies. Especially for the last two industry sectors, cells with high reliability and long lifetimes are essential. Those cells are often in the range of several ampere hours as they are strategically used to reduce construction effort due to a large number of cells and to increase energy density.

In order to ensure reliability and good performance over lifetime, the aging of the cells needs to be well understood. Thus, a wide range of temperatures, current rates, states-of-charge (SOC) and depths-of-discharge (DOD) of the application should be

* Corresponding author. Electrochemical Energy Conversion and Storage Systems Group, Institute for Power Electronics and Electrical Drives (ISEA), RWTH Aachen University, Jägerstrasse 17/19, D-52066, Aachen, Germany.
E-mail address: mlw@isea.rwth-aachen.de (M. Lewerenz).

Abbreviations

FCE	full cycle equivalents
DVA	differential voltage analysis
EC	ethylene carbonate
DMC	dimethylene carbonate
EMC	ethylene-methylene carbonate
DEC	diethylene carbonate
LFP	lithiumironphosphate
SEI	solid electrolyte interphase
DOD	depth-of-discharge
SOC	state-of-charge

covered by the aging tests. In literature there are many different test matrices for different cell types. Those cell types are specified by their electrode chemistries, electrolyte composition, their amount of capacity, their shape and coating optimization for high power or high energy performance [1–6].

Finally, it is hardly possible to compare test results of different cell designs just by capacity fade and increase of internal resistance. Therefore the aging effects need to be assigned to some specification of the cell to be able to generalize. There are only few large test matrices for LiFePO$_4$|Graphite cells reported in literature comprising calendar life tests and cycle life tests for cylindrical cells with capacities that are significantly larger than the consumer size of 18650, e.g. in Refs. [4,7].

To our knowledge, many effects with respect to surprisingly increasing or decreasing extractable capacities have been described in literature that are not well understood. For instance an effect often called *refresh effect* has been observed where the capacity is rising in the order of up to 5% at the start of the test instead of an intuitive monotone decreasing trend [2], or where the linear-like capacity fade seems to start after 50 days of aging, which can be seen in Fig. 6 of Ecker et al. [1].

Furthermore changing the SOC during a test may lead to a spontaneous capacity increase or decrease in the order of up to 5% or higher for small-sized cells. As an example Käbitz et al. raised the question in their publication (Fig. 13 in Ref. [2]) why at 40 °C and 60 °C an offset of about 5% occurs in the capacity trend between storing the cells at 50% and 20% SOC where the offset is in the same order of magnitude for both temperatures. In addition to the aging at three fixed SOCs, they also performed the aging of a cell that switched between different SOCs for different period lengths (Fig. 15 in Ref. [2]). This test exhibits an additional increase of capacity at 20% SOC and decrease for 50% SOC and higher while the decrease is strongest at 100% SOC. They showed that this increase or decrease of capacity seems to be reversible and the amount of the recovered capacity is increasing with time.

This effect is observable as well if a test is interrupted at a SOC which is strongly deviating from the mean test SOC for some reason. In this case a capacity refresh or stronger decrease is expected, which will go back to the expected capacity fade trend asymptotically. In the work of Reichert et al. the capacity relaxation after two hours rest during full cycle tests has been investigated [8]. They found out that this relaxation is in the order of 0.1% of the measured capacity and that it has no influence on aging of different types of cells. The temperature dependency between 20 and 40 °C is low but the relaxation effect at 10 °C exhibits nearly no relaxation effect. A five days' rest leads to a capacity increase of 0.5 Ah which is reached asymptotically.

Those trends cannot be fully explained with current simulation models of lithium-ion batteries. They are, however, explainable understanding *the passive electrode effect* which takes the geometrical oversized anode compared to the cathode into account. Recently a publication of Gyenes et al. [9] was published that shows this effect focusing on the post-mortem analysis and Coulombic efficiency. Considering this effect means that it will affect e. g. test protocols, modelling of aging, online diagnostics and self-discharge measurements. This effect will be explained and discussed in this contribution.

In the framework of this publication the dependency of capacity losses and the increase of internal resistances with respect to temperature, SOC, C-rate and DOD of 50 cylindrical 8 Ah LiFe-PO$_4$|Graphite cells are discussed. The rise of capacity above the initial values within the first cycles is explained. Thus, an SOC-dependent effect is influencing especially the capacity trend of the calendaric aging tests as the cyclic aging tests refer to no fixed SOC and are conducted symmetrically around 50% SOC. The results will be validated by post-mortem analyses of selected cells with the focus on cells showing an exceptional behavior. The lifetime tests discussed in this publication form the base for subsequent publications discussing the results of non-destructive analyses like differential voltage analysis (DVA), evaluation of capacity differences of capacity measurements at 1 C and 0.25 C and floating currents.

2. Experimental

Cylindrical 8 Ah cells with lithiumironphosphate (LFP) on the cathode, graphite on the anode and (EC-DMC-DEC-EMC)-LiPF$_6$ electrolyte were tested using different test stations of the brand Digatron (MCFT 20-05-50ME, MCT 50-06-12ME and MCT 100-06-12ME with precision of current measurement of 0.1%). The temperature sensor AD 590 with a precision of ± 1 K is located on the cell case. The cell tests are conducted in temperature chambers made by Binder (MK53, MK240 and MK729 with temperature precision up to ± 2 K) and 110 l ovens by Memmert (temperature precision up to ± 0.5 K). The tests are divided into calendaric and cyclic aging tests. The specifications of the cell are given in Table 1. As current rates for charging up to 10 C are within the specification, the cell can be accounted as a high-power cell.

In the following DOD is used in terms of cycle depth always with respect to the nominal capacity. The SOC of cyclic aging tests represents the mean SOC during cycling. The *initial open circuit voltage (initial OCV)* represents the OCV measured at the cells prior to testing.

The calendaric aging was performed at 25 °C, 40 °C and 60 °C and at 20%, 50%, 80% and 100% SOC (Table 2). Only the 100% tests were floated at a voltage of 3.6 V, as the voltage curve at a lower SOC is too flat to fix the SOC by a certain voltage in a practical setup. All other test SOCs are approached Ah-based and remain in the temperature chambers at open circuits. Every 14 days a full check-up was performed. The check-up periods were reduced for slow aging conditions during testing time. At each check-up a capacity test and a pulse-current test were performed. A detailed description of the check-up is given at the end of this chapter.

The cycling aging was split into two batches (Table 3): The first

Table 1
Specifications of the test cell.

Head	M6
Diameter	38.5 mm
Length w/o terminals	121 mm
Mass	310 g
Max. Conti. charge/discharge current	10 C/80 A
Operation temperature range (cycling)	0-45 °C

Table 2
Matrix of calendar aging test and the number of cells for the corresponding test. The tests at 100% SOC have been floated at 3.6 V. During check-up the temperature is reduced to 25 °C.

SOC	25 °C	40 °C	60 °C
20%		3	
50%	3	3	3
80%		3	
100%	3	3	3

Table 3
Matrix of cyclic aging test and the number of cells for the corresponding test. All cycling tests have a mean SOC of 50%. The temperature chamber was adjusted to ensure a cell temperature of 40 °C measured at the cell case. During check-up the temperature is reduced to 25 °C.

C-rate	Depth-of-discharge		
	100%	50%	10%
1 C	3	9	3
2 C		3	
4 C		3	
8 C		5	

at different C-rates and the second at different DODs. The first test was performed at 1 C (8 A), 2 C (16 A), 4 C (32 A) and 8 C (64 A) between 25 and 75% SOC (50% DOD). The second test was performed with 10% DOD (45–55%), 50% DOD (25–75%) and 100% DOD (0–100%) at 1 C. Each test condition was applied to 3 cells respectively. Only the test at 1 C, 25–75% SOC comprises 9 cells to be able to evaluate the cell reproducibility with a higher statistic at moderate aging conditions.

After a complete charge the mean SOC of the corresponding cycle, defined using the current capacity, was approached Ah-based as LiFePO$_4$ is featured by a very flat open circuit voltage (OCV) curve. The only exception is the 1 C 100% DOD test, which needs to be conducted voltage-based. The cells are cycled Ah-based around the mean SOC of the cycling and the DOD is related to the nominal capacity, i.e. the DOD is not adapted to the current capacity. The cycled cells are all kept at a temperature of 40 °C of the cell's case in a temperature chamber. To keep the temperature of cell's case at 40 °C, the temperature of the chamber needs to be kept at 40 °C or lower, depending on the resistive heat generated by cycling with the according C-rate and aging-dependent internal resistance. The generated heat becomes significant from 2 C on, so the temperature of the chamber is reduced from initially 38 to 36 °C at 2 C, 31 °C at 4 C and initially 24 to 22 °C at 8 C.

After every 100 full cycle equivalents (FCE) the tests were interrupted for a check-up. Due to setup constraints the 2 C-test check-ups were performed after 200 FCE. In the check-up the temperature is set to 25 °C until a homogenous temperature within the cells is established. Due to the tolerance of the temperature chamber cell surface temperature window of all cells is in the range of 25–27 °C. Within the check-up a capacity test and a pulse-current test are executed.

During the check-up cells are first discharged down to 2.0 V is reached, then charged with 1 C (8 A) up to 3.65 V, followed by constant-voltage charging up to I < 0.05 C (maximum 2 h). Afterwards the cells rest for 30 min before discharging with 1 C (8 A) until the voltage of 2.0 V is reached. The latter discharge is used for 1 C capacity determination.

The pulse test is executed after a 30 min rest period at a SOC of 50% with respect to the actual capacity. The pulse test itself consists of 18 s at 2 C discharge pulse with 40 s rest period and followed by a 10 s at 1 C charge pulse with subsequent 40 s rest time. The pulse

tests are evaluated in this publication after 10 s at 50% SOC for discharge and referred to as internal resistance in the following sections. They mainly reveal information about ohmic losses and charge transfer resistances.

The post-mortem analysis is performed under argon atmosphere. The cells are evaluated by their surface morphology using a Keyence VK-9710 laser microscope (confocal microscope) and the amount of metal is quantified measuring electrodes solved in aqua regia with Varian 725 ICP-OES (Inductively Coupled Plasma-Optical Emission Spectroscopy).

3. Results and discussion

3.1. Initial tests

The initial tests reveal that all cells have a higher capacity of 2–12% compared to its nominal capacity of 8 Ah and the internal resistance is in the range of 6.5–9 mΩ. Even though the spread in initial capacity and internal resistance is comparably high, no significant influence regarding the behavior on the following aging tests could be observed.

In Fig. 1 the designs of the overlap in the rolled anode and cathode are sketched to illustrate the distribution of the overhang of the anode. Due to positioning tolerance of both electrodes one electrode is exceeding the other in height. In most cases the exceeding electrode is the anode to minimize risk of plating at the edges of the overhang. Additional overhang is originated from the winding over the rod in the core of the jelly roll for stability reasons and because of the fact that due to the double-sided coating the very last anode part at the outside of the jelly roll has no counter cathode. The exceeding part of the anode is further discussed as *passive anode* as this part is not directly charge- or dischargeable via the cathode. The overlap of cathode and anode will be named on the anode side as *active anode*. The share of the overhang for this cell is calculated in a good approximation as follows:

$$Share\ of\ Overhang = \frac{l_{anode} \cdot h_{anode} - l_{cathode} \cdot h_{cathode}}{l_{cathode} \cdot h_{cathode}} = 5.7\%$$

where l is the length and h the height of the corresponding electrode.
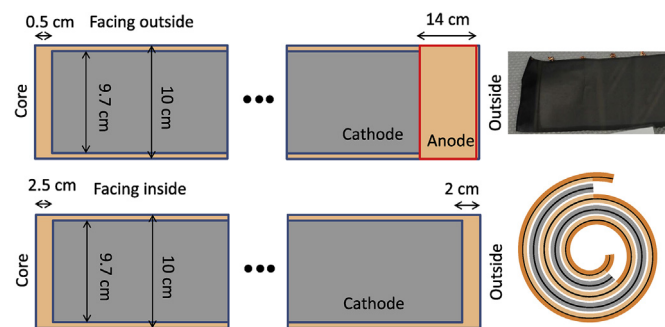

Fig. 1. Sketch of the dimension of the overlap of the rolled jelly roll measured during a post-mortem analysis. Grey represents the cathode and orange the geometric excess anode. The top sketches the outward view and bottom the inward view. The left part represents the core of the jelly roll and the right part the very last windings of the jelly roll. The 3 mm differences in height are due to positioning tolerance between anode and cathode. In the lower right the top view of a schematic winding is shown. In the core the anode only is winded over a rod. The last winding of the anode has due to the double-sided coating no counter cathode and is the biggest area of passive anode and is slightly longer than one complete winding. The overlap is eye-catching due to the different color compared to the active part of the anode illustrated in the photography in the upper right. The total length of the unrolled anode is 369 cm and of the cathode is 360 cm. (For interpretation of the references to colour in this figure legend, the reader is referred to the web version of this article.)

3.2. Calendaric aging

3.2.1. Results of calendaric aging

After more than 2 years and 25 check-ups the storage tests at 25 °C showed no increase, rather a decrease of about 10% in internal resistance and a capacity loss that is about 1−2% of the initial capacity (Fig. 2 top). Within the first 200−400 days the capacity is increased by about 0.7−1.3% of the initial capacity before the capacity loss due to aging becomes measureable. The low aging with respect to capacity fade and increase of internal resistance implies that there is very low calendaric aging at 25 °C and thus the check-ups themselves do hardly contribute to cell aging.

The cells stored at 40 °C show a SOC-dependent trend during the first capacity tests that is followed by a rather linear capacity decrease (Fig. 2 middle). At 20% SOC a strong and at 50% a weaker trend of capacity rise over 200 days is recognizable. At 100% and 80% only a slight difference between the first and the second check-up is measured.

The internal resistance is decreasing or stays below 110% of the starting value which is in good correlation to Zhang et al. [4]. Only one cell in the 80% SOC test rises to about 20% increase of internal resistance. Nothing else in particular could be found for this cell. Generally the measurement of internal resistances returns a few data points that do not follow the overall trend. This corresponds to the high sensitivity to temperature changes during the check-up tests and is not related to aging. With the exception of one cell at 20% SOC the test results are reproducible for the three cells in every test condition concerning capacity loss. The deviating behavior of this cell is visible in the first check-ups, while the subsequent linear characteristic is comparable. No clear explanations for this phenomenon could be found.

In contrast to the tests at 25 °C and 40 °C the tests at 60 °C do show a considerably high capacity fade and a low reproducibility of the three cells under the same test conditions (Fig. 2 bottom). Furthermore the capacity fade is not following a linear behavior and is decreasing with aging.

Looking at all three temperatures the internal resistance reaches a higher value with higher temperatures. Thus comparing 50% and 100% SOC at 25 °C the internal resistance is reduced; at 40 °C it is slightly reduced or constant and at 60 °C the internal resistance is rising.

3.2.2. Discussion of calendaric aging

In this section the SOC-depending part of the capacity graphs is discussed at first as this trend is related to a reversible capacity loss or increase and needs to be separated from the irreversible capacity loss. This effect is called passive electrode effect. In the subsequent chapter only the irreversible part of the capacity fade and the internal resistance are discussed.

3.3. Passive electrode effect

In this chapter the theory to explain the initial part of the capacity trend (including the capacity rise in early stages of life for cells stored at certain SOCs) shown in Fig. 2 can be found in the geometric excess anodes compared to the cathodes, i.e. the part of the anode which has no counter electrode (cathode). The principle of this theory is sketched in Fig. 3. Before starting our tests the OCV for all cells was exactly at 3.34 V, which corresponds to a SOC of about 99% and an OCV of 88 mV of graphite vs. lithium. The link of graphite vs. lithium and the SOC of the full cell are found by correlating the positions of the voltage transitions of the graphite in
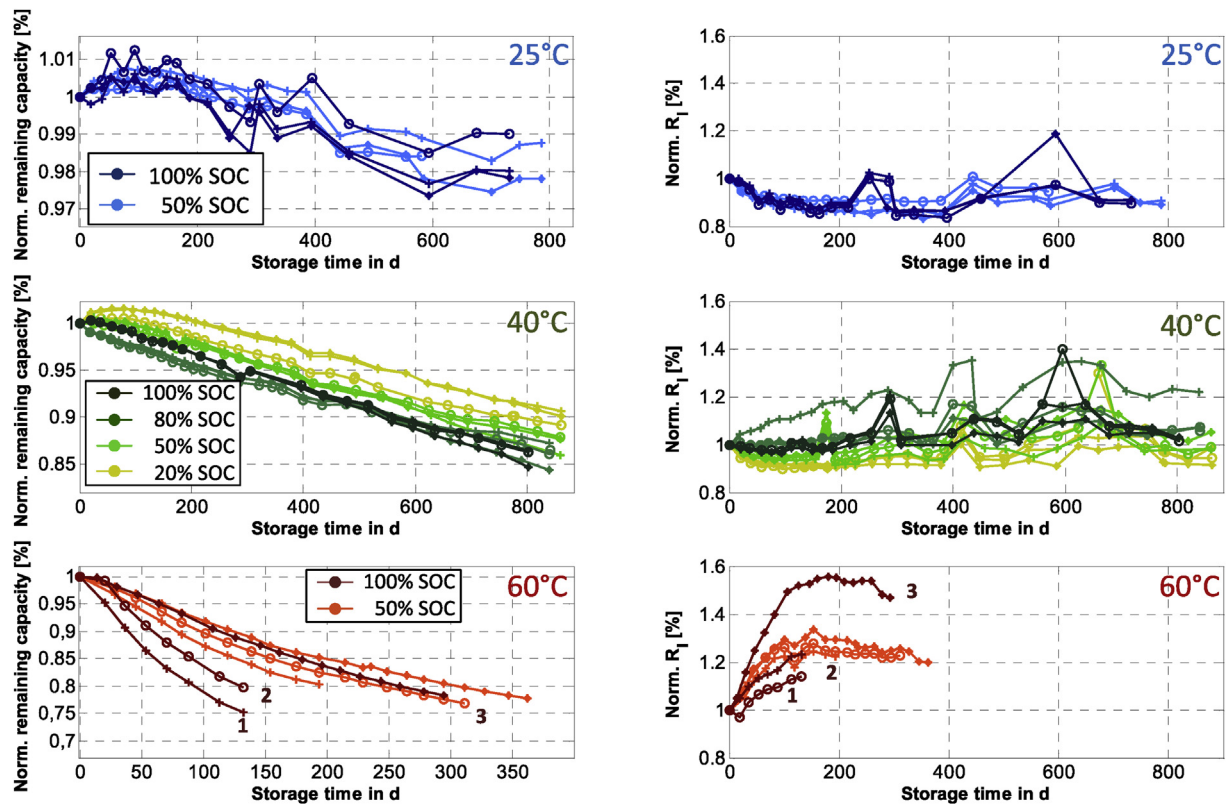

Fig. 2. Illustration of the remaining capacity normalized to the initial capacity (left) and the internal resistance at 50% SOC normalized to the initial resistance (right) of all 3 cells of each calendaric test at 25 °C (top), 40 °C (middle) and 60 °C (bottom). (For interpretation of the references to colour in this figure legend, the reader is referred to the web version of this article.)
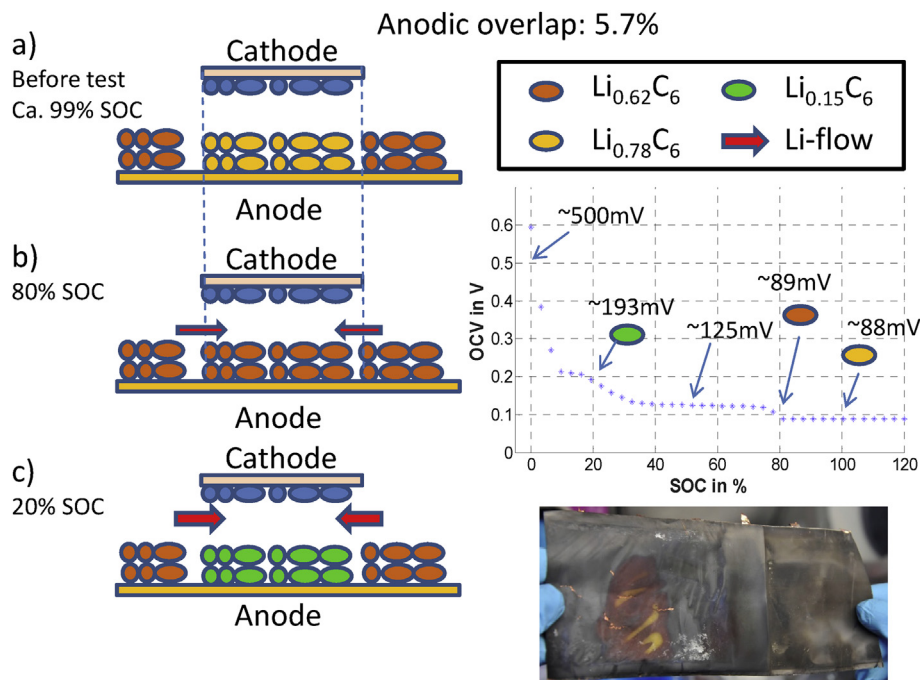
Fig. 3. Sketch of the theory to explain the SOC-depending capacity trend of the first few cycles. In a) the cell was stored before test at a SOC of about 99% for a long time before our tests started. The passive anode is charged by the active anode until the potential difference is equalized. This is the case at 80% SOC on the passive anode. In b) the cell is discharged in the active part to 80% SOC. Lithium is not transported from the passive to the active anode as the voltage differences are too small (<1 mV). In c) the cell is discharged to 20% SOC in active anode. The potential difference between the active and passive anode is now higher (105 mV), which leads to a significant lithium transport. The anodic potentials at 20%, 50%, 80% and 100% are given in the OCV plot of the anode vs. lithium. In the lower right part a photo of a passive anode which is situated at the very outside (part within the red rectangle in Fig. 1) that exhibits colors from gold to black that is linked to state-of-charge. (For interpretation of the references to colour in this figure legend, the reader is referred to the web version of this article.)

half-cell and full-cell voltage curves. As the OCV itself does not correspond to a precise SOC due to hysteresis of the LiFePO$_4$ as reported by Marongiu et al., the necessary residual charge until 100% SOC has been evaluated for its determination [10]. Now the passive anode is charged by the active anode until the potential difference is equalized which is the case at about 80% SOC due to the very flat plateau of the anode potential vs. lithium. If the cell is now kept at lower SOCs of the full cell during a storage test corresponding to higher electrode potentials of the anode vs. Li/Li$^+$, lithium-ions move towards the active anode and active lithium is gained leading to an increase in capacity. If the OCV of the passive anode before the test would be lower than the OCV of the storage test even lithium loss towards the passive anode is expected. The lithium-ion flow is especially strong if there is a high potential difference. This is the case for SOCs lower than 75–80% (Fig. 3). Thus at SOCs above 80%, the low potential difference within a plateau leads to an extremely slow equalizing flow of active lithium. This flow rate will be hardly recognizable in capacity fade as the flow of lithium-ion will be too low. Absolute values to describe the flow of active lithium will be the subject of future projects.

Thus there is nearly no potential difference between 100% and 80% which should result in no initial negative or positive trend of the capacity loss in this SOC range. This is in accordance with the results of Gyenes et al. [9] as they showed that the anode overlap reveals a red color (ca. 80% SOC) and the active part was golden (ca. 100% SOC). At 50% SOC there is a potential difference of about 37 mV meaning that a low initial increase of capacity should be measurable. Finally at 20% the strongest increase should be measureable as the potential difference reaches about 105 mV. The previously described potential differences ΔOCV(max) at the corresponding test condition between the passive and the active anode at begin of test are summarized in Table 4.

Assuming that the initial capacity rise is reversible the flowing linear trend is evaluated by a linear regression. The percentage increase or decrease ΔC_{rel} is calculated by extrapolating the linear trend to t = 0 days. The initial trend shows a high capacity increase for tests at 20% SOC of 1.5–3.4%, a slight capacity increase for 50% SOC of 0.6–1.7% and for 100% SOC of 0.5–0.7%. The tests at 80% SOC exhibit a 0.7% decrease. The results are summarized in Table 5.

Now a simple calculation follows to prove the measured results with the given theory. As a result of a post-mortem-analysis the geometric excess anode is 5.7% of the full active anode area (Fig. 1). Thus, as the SOC of the passive anode is 80%, about a ΔSOC of 60% of the lithium could be extracted from the passive part at 20% SOC storage condition and about ΔSOC = 30% in the 50% SOC storage condition (Table 5). In total $\Delta C_{Theo}^{rel} = 5.7\% \cdot 60\% = 3.4\%$ for 20% SOC and $\Delta C_{Theo}^{rel} = 5.7\% \cdot 30\% = 1.7\%$ for 50% storage condition are extractable. As the 50% SOC storage is within the middle plateau of the anode, ΔC_{Theo}^{rel} might even be lower as the potential differences between passive and active anode close to 50% SOC become very

Table 4
OCV cell voltage of the full cell and initial maximum potential difference between the passive anode of 99% SOC and the active anode at the corresponding SOC of the test.

		Full cell OCV @test	ΔOCV(max)@anode
25 °C	50%	3.29 V	37 mV
	100%	3.60 V	0 mV
40 °C	20%	3.20 V	105 mV
	50%	3.29 V	37 mV
	80%	3.33 V	0 mV
	100%	3.60 V	<1 mV
60 °C	50%	3.29 V	37 mV
	100%	3.60 V	0 mV

Table 5
ΔC_{rel} represents the expected initial capacity for the 3 cells at each test condition after the flow of all lithium according to positive electrode effect is concluded. These values are well matching to the simply derived values $\Delta C_{rel}^{Theo.}$ according to the positive electrode effect and corrected by the deviations due to testing $\Delta C_{rel}^{Testing}$.

		ΔC_{rel}				ΔC_{rel} Theo.	$\Delta C_{rel}^{Testing}$
		Cell 1	Cell 2	Cell 3	Avg.		
25 °C	50%	1.2%	1.2%	1.3%	1.2%	1.7%	
	100%	1.0%	0.7%	1.1%	0.9%	0%	0.8%
40 °C	20%	1.5%	3.1%	3.4%	2.7%	3.4%	
	50%	1.7%	0.6%	1.0%	1.1%	1.7%	
	80%	−0.7%	−0.7%	−0.7%	−0.7%	0%	−0.7%
	100%	0.5%	0.5%	0.7%	0.6%	0.8%	0.8%
60 °C	50%	0.7%	0.6%	0.4%	0.6%	1.7%	
	100%	0.4%	0.9%	1.0%	0.8%	0%	0.8%

low.

Although the measurement results agree with this theory for 20% and 50% SOC quite well, the cells at 100% SOC do show an unexpected increase and at 80% SOC an unexpected decrease of capacity. Still this is explainable by looking closer at the test protocols. As there were problems with data logging of the 80% cells, the tests were interrupted before the first check-up for 1 week at a state-of-charge of 20% which leads to a lithium-ion flow towards the active part of the anode. So in the following first check-up a higher capacity could be measured. This explains the initial drop between the first and the second capacity measurement of the 80% SOC storage test by its near prehistory. The prehistory is also important for the cells stored at 100% SOC as the initial standard 1 C charge of the check-up results in an OCV of 3.36–3.37 V for the very first capacity test. But the cells stored at 100% SOC test are floated at 3.6 V which is finally the OCV of the cell before the check-up. The following capacity tests start now from 3.6 V instead of 3.36–3.37 V. The difference in Ah between 3.6 V OCV and 3.36–3.37 V is about 0.06 Ah or 0.8% of the nominal capacity. This approach matches well with the observed increase in capacity at 100% SOC (Table 8). The tests at 25 °C and 100% SOC reveal similar results with 0.7–1% capacity increase. All results including testing peculiarities $\Delta C_{rel}^{Testing}$ are summarized in Table 5.

In fact this is a simplified approach which is very sensitive to test procedure including test interruptions. The approach does not take into account the electrical disconnection of particles or inhomogeneous distributions. Furthermore some parts of the passive anode are closer to the active part and will participate faster than others and the aging of the passive anode is not understood so far.

The strength of this theory is that it can be generalized at least for all graphite-based anodes comprising a geometric excess anode, wherefore a validation of this theory by using different electrolytes and cathode materials is recommended. An initial OCV prior to test begin that corresponds to a lower SOC than the storage SOC could even prove the postulated loss of active lithium from the active anode. As this effect will be valid for an oversized cathode as well, it should be called: Passive Electrode Effect.

This initial trend in degradation curves can be seen in many publications while mostly the change in capacity loss is evaluated without discussing the SOC-dependent strong increase or decrease at the beginning of the test [1,11]. Unfortunately, information on the SOC, the cells stored prior to the aging test, and the percentage of the excess anode are not stated in those publications which would enable verification of the theory with respect to their data. To be able to interpret the tests, the amount of excess anode compared to the cathode and the initial SOC prior to start of the test need to be stated in not only publications, but as well in data sheets for batteries, since this will significantly influence the capacity loss according to the application.

Furthermore the capacity increase, e.g. after a longer interruption of testing or after changing the storage SOC, can be explained in numerous cases by this theory. For instance this is the case for Reichert et al. [8]., where short-term relaxation times are tested as reported before. While the relaxation was measured at 0% SOC, it will lead to a high potential difference between passive and active anode for most SOC of the passive anode. Reichert et al. already found out that this relaxation effect (due to the passive electrode effect) starts to be temperature-dependent below 20 °C. Deviations between the NMC and LFP cell might result in different initial SOC prior to testing. Finally they confirm the findings of Käbitz et al. [2] by highlighting that this effect is of reversible nature and is not corresponding to aging.

In fact this theory may have an impact on the assumption that calendaric aging is following a $\sqrt{t}$-trend as well, which is proposed by Ploehn et al. [12] and Broussely et al. [13]. They motivate this by the protective nature of a growing SEI layer with the square root of time. The initial SOC prior to testing is for most lithium-ion cells at very low SOC of 40% or lower. Therefore, at least for higher SOCs, a stronger capacity decrease is observable in the very beginning, which might lead to the assumption of a $\sqrt{t}$-correlation. This is the case for the publication of Broussely et al. where calendaric aging tests on $LiCoO_2$, $LiNiCoO_2$ and $NiMnO_2$ vs. graphite are evaluated [13]. Here the initial trend is observed within the first 100 days while the storage voltage is always higher than 3.8 V which corresponds to SOCs above 60%. However, knowing the passive electrode effect a rather linear trend might be more likely according to the data, assuming a low aging rate. Finally this simple observation does not raise a claim to cope with a profound aging model.

3.4. Capacity and resistance

According to the findings presented in the previous chapter the initial rise of capacity is a reversible effect. Thus the slope of the linear part at the end of tests returns with a good approximation the aging which is strongly related to the loss of active lithium. Therefore the slopes of the linear characteristics are evaluated to display the cells' aging. The results for all tests are given in Table 6.

At 25 °C at 50% and 100% SOC no different slope of the linear characteristic is observable. Thus there is no measurable dependency with respect to SOC. According to the slope of the linear characteristic of the capacity fade of the 40 °C tests, the aging is more or less constant for 20% (3.20 V), 50% (3.29 V) and 80% SOC (3.33 V) and slightly increased for 100% SOC (3.60 V) by 15–20%, which might be explained by the approximately 300 mV higher storage potential of the full cell. As the anode is very flat at higher SOCs, this additional potential is originated from the positive electrode. Therefore an aging corresponding to the cathode is likely but could not be proved by post-mortem analysis, as no significant

Table 6
Slope of the linear regression y = (100% + ΔC_{rel}) - x dC_{rel} dt^{-1} after the initial trend and before aging becomes non-linear. As the initial trend is a reversible effect the slope represents the actual capacity fade.

		dC_{rel} dt^{-1} in % $(100d)^{-1}$		
		Cell 1	Cell 2	Cell 3
25 °C	50%	0.4	0.5	0.5
	100%	0.4	0.3	0.5
40 °C	20%	1.5	1.5	1.5
	50%	1.8	1.5	1.6
	80%	1.5	1.5	1.7
	100%	1.8	1.8	2.0
60 °C	50%	>10.6	>12.4	>8.6
	100%	>26.3	>17.9	>9.4

difference with respect to the Fe-content could be found measured by ICP up to 40 °C.

The roughly 10% improvement of the internal resistance of the 25 °C test cells within the first 50−100 days might be originated from the slow cycling during check-up after a long storage time before test begin. Potentially the lithium and electrolyte distribution is better with respect to internal resistance compared to a cell that is stored for a long period. This effect will be superposed to all tested cells. Käbitz et al. found out in their work that the internal resistance is lower for cycled than for calendaric aged cells at 25 °C [2]. However no explanation could be found in literature for the reducing internal resistance. The cells tested at 40 °C exhibit a decreasing of the internal resistance for 20% and 50% SOC while the internal resistance remains rather constant at 80% and 100% SOC. Although no Fe could be found in disassembled cells at 80% and 100% SOC, the Fe dissolution might be present in lower quantities that are below the resolution of the ICP.

Although the 60 °C test cells do not follow a linear behavior, the linear regression was conducted to compare the values in Table 6 with the results of the 25 °C and 40 °C tests. Therefore only the 3rd to 6th checkup-ups are evaluated. Thus the overall aging rate will be higher as stated and the results suffer from higher uncertainties.

Neglecting cell 3 of the 100% tests for the first instance because of its very special behavior, the capacity fade is increasing with higher SOC and the trend of the internal resistance is rather SOC-independent. The internal resistance is increasing and is turning to be constant after 100−150 days of aging for all cells stored at 50% SOC. Unfortunately this observation cannot be fully approved for the cells 1 and 2 of the 100% SOC test as their aging time is not exceeding 150 days. As up to 40 °C the internal resistance remains nearly constant, it might be possible that at 60 °C within the first 100−150 days another aging mechanism is dominating the increase of internal resistance.

A leakage of the cells can be excluded as an aging mechanism as the deviation in weight before and after the test is smaller than 0.2 g which is in the order of the accuracy of the balance.

A simple explanation might be residual moisture even in low quantities that leads to strong decomposition of $LiPF_6$ at temperatures of 50 °C and higher until the moisture has fully reacted, which is reported by Lux et al. [14] or alternatively the residual moisture could also dissolve Fe from the cathode active material which is dominant at elevated temperatures like 60 °C as summarized by Dubarry et al. [15] and Klett et al. [6]. Considering this theory, different amounts of moisture within the cell due to variation in manufacturing conditions could significantly affect the aging of each individual cell.

In post-mortem analyses for some cells the Fe-content has been measured spatial resolved using the ICP-OES (Table 7). Up to 40 °C no significant increase above the measurement noise is observed. At 60 °C Fe can be measured from 0.1 to 0.7% of the total Fe present in the cathode active material. At 50% SOC and 60 °C only 0.1%% are measured for both disassembled cells, whereas at 100% SOC and 60 °C values of 0.4% and 0.7% are measured, which correlates to the different trend of capacity fade.

This might be an explanation for the extraordinary behavior of

Table 7
Measurement results of the mean values of Fe content at the anode aged at 60 °C.

	Cell	Fe content in $\mu mol\ cm^{-2}$	Share of Fe in cathode
Fresh cell		0.03	0.02%
60 °C-50% SOC	1	0.13	0.1%
	3	0.15	0.1%
60 °C-100% SOC	2	0.45	0.4%
	3	0.97	0.7%

cell 3 of the 100% SOC storage test. This cell exhibits a comparably low capacity fade and the highest increase of internal resistance to about 150% of its initial value. This is a good example to illustrate that an increase to 150% of the initial internal resistance does not negatively affect the cell's capacity at 1 C. Nevertheless the internal resistance turns to be constant after 100−150 days as well, which seems to indicate that the aging mechanism is comparable to the other cells aged at 60 °C. If this cell would have contained a reasonably higher amount of moisture than the other cells, the internal resistance would increase more as the moisture is reacting with the electrolyte to form solid electrolyte interphase (SEI). A good understanding why cell 3 reveals the lowest capacity fade and the highest resistance is not understood by the authors. Unfortunately this theory cannot be proved or disproved easily as for example the amounts of moisture at begin of test are not measurable.

More details are made available by evaluating the floating currents of the 100% SOC tests in a publication that is currently under review [16]. There the floating currents keeping the 3.6 V of 100% SOC tests are logged and related to the derivative of the pure capacity loss. In an Arrhenius representation the floating currents for temperatures between 25 and 65 °C are evaluated. The plot returns two different dominating processes above and below 45 °C. Thus, at temperatures greater than 45 °C an aging mechanism is dominating that apparently leads to an increase of internal resistance.

3.5. Cyclic aging

3.5.1. Results cyclic of aging
The cells aged at 50% DOD in the range of 25−75% SOC are shown in Fig. 4. The cells mostly show aging in form of capacity fade. The corresponding internal resistance is only increased for special aging conditions, e.g. cells tested at 8 C and after high capacity loss of 30−40%. At C-rates of 8 C the internal resistance increases faster after reaching the cut-off voltage (Fig. 4 bottom right). The increase of internal resistance of 20% is still in the initial deviation of the cells of 6.5−9 mΩ of about 30%.

Down to a remaining capacity of 80% the cells last from 1000 to 4800 FCE and show a maximum internal resistance of 95−120%. Neglecting the strongly aged 2 C cell and the 8 C aged cells, the cells last from 2000 to 4800 FCE and show no increase in internal resistance (95−100%).

The cells refer to a linear-like capacity decrease while the slope especially for 8 C tests is increasing if the extractable capacity is lower than 8 Ah during cycling starting from 1500 to 2000 FCE. Assuming linear aging down to remaining capacities of 80%, the slopes of the capacity fade are evaluated and stated in Table 8. The reproducibility of the 9 cells at 1 C 50% DOD down to 80% remaining capacity is given by the average value and by the standard deviation: $(6.1 \pm 0.6)\% \ (1000\ FCE)^{-1}$.

The results of the cells aged at 1 C at 10%, 50% and 100% DOD do not show a straight forward DOD-dependence where higher DOD corresponds to higher capacity fade (Fig. 5). Whereas the aging rates at 50% and 100% DOD are quite comparable, the cells cycled at 10% DOD are aging significantly faster with respect to capacity fade and increase of internal resistance which is eye-catching looking at the slopes in Table 8. Here cycling until the cut-off voltages are reached does not lead to faster capacity fade or increased internal resistance as reported before for higher C-rates. Only cell 3 at 1 C 100% DOD reveals a stronger aging from 5500 FCE on, correlating with an increase of internal resistance (Fig. 5).

3.5.2. Discussion of the cyclic aging
As already shown for the calendaric aging tests the capacity fade and the increase of internal resistance do not directly correlate for
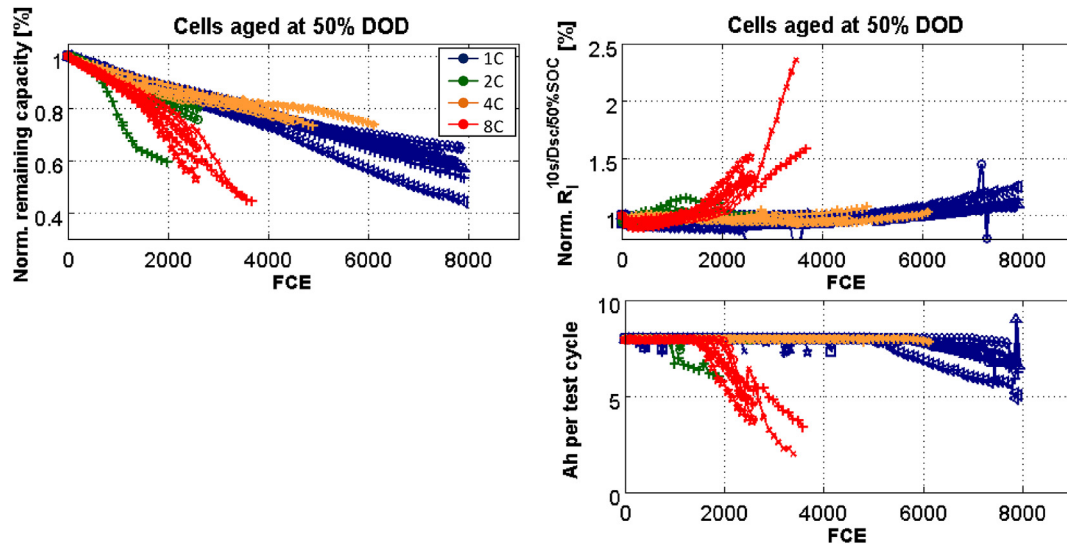
Fig. 4. Trend of the relative capacity (top left) and the internal resistance (top right) of the cycle aging tests at 50% DOD and C-rates of 1 C, 2 C, 4 C and 8 C at 40 °C cell temperature. The internal resistance correlates with Ah cycled per cell (bottom right). If the Ah per cycle is lower than 8 Ah the cut-off voltages are reached and the cells are cycled voltage-based. (For interpretation of the references to colour in this figure legend, the reader is referred to the web version of this article.)

Table 8
Comparison of the cyclic aging rates evaluated down to 80% remaining capacity by assuming a linear behavior for easier comparison. $y = A - x \, dC_{rel} \, dFCE^{-1}$.

	DOD	$-dC_{rel} \, dFCE^{-1}$ in % 1000 FCE^{-1}			Annotation
		Max	Avg	Min	
1C	10%	10.0	9.9	8.7	Aging faster than linear
	100%	7.6	6.4	5.5	
	50%	7.1	6.0	5.0	
2C	50%	10.2	9.2	8.2	Extraordinary cell 1 excluded
4C	50%	5.4	4.7	3.7	
8C	50%	12.7	11.3	9.6	After 80% higher slope

the cyclic aging as well. However, if the capacity loss is increasing stronger than linear, the internal resistance is rising simultaneously. Thus the additional losses correlate to the increase of internal resistance.

Despite the higher C-rate the cells aged at 4 C show a comparable capacity fade with respect to the cells aged at 1 C, whereas the cells aged at 2 C show a significantly faster aging. This might be explained by increased core temperature of the cell at higher C-

rates due to resistive heat generation. The heat generation can be estimated considering the chamber temperatures of the corresponding tests keeping the surface temperature of the cell constant as discussed in the experimental part before. Thus aging conditions at 1 C are low and the generated heat at 1 C is low as well. At 2 C the aging conditions are stronger but still the heat generation is rather low, whereas at 4 C the heat generation might be strong enough to homogenize the discharging and reduce overpotentials which finally lead to a more homogeneous and less severe aging. At 8 C the temperature seems to reach a crucial limit and different aging effects might lead to the non-linear aging.

The capacity fade for aging at 1–4 C does not always follow a strictly linear behavior. The capacity loss for some cells behaves partially linear with different slopes while the slope is sometimes increasing or sometimes decreasing. This behavior leads to the assumption that certain aging processes are very disjunct and occurring successively. These processes start at a certain time and are completed abruptly. They do not seem to fade out for a longer period. Two examples at 2 C and 4 C are highlighted in Fig. 6.

A post-mortem-analysis of the strongly aged 2 C cell exhibits the formation of a dense cover layer that is linked to increasing slope of capacity fade until the formation of the dense layer is completed.
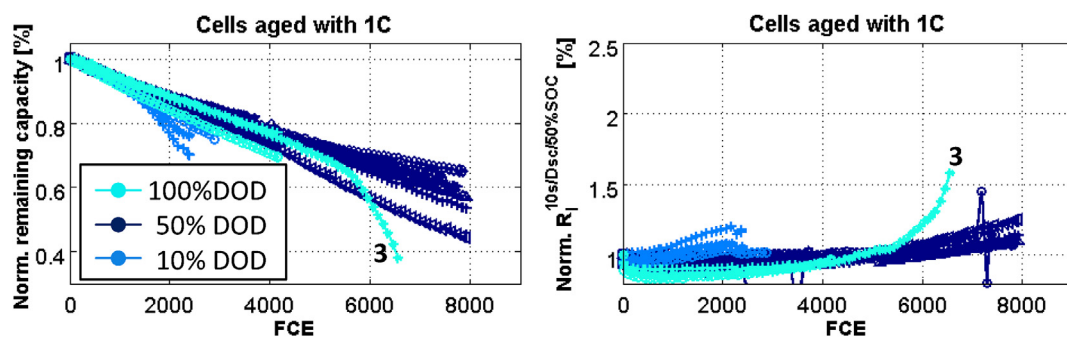

Fig. 5. Trend of the relative capacity (left) and the internal resistance (right) of the cycle aging tests at a C-rate of 1C for 10%, 50% and 100% DOD with respect to a mean SOC of 50% and 40 °C cell temperature. (For interpretation of the references to colour in this figure legend, the reader is referred to the web version of this article.)
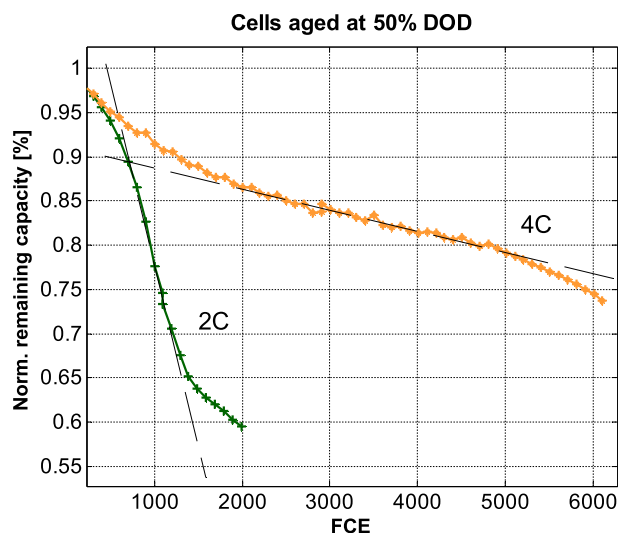
Fig. 6. Special characteristics of capacity fade of a 2 C (cell 1) and a 4 C (cell 3) test cell aged between 25 and 75% SOC. The cells are featured by different linear phases from higher to lower aging rates and vice versa. (For interpretation of the references to colour in this figure legend, the reader is referred to the web version of this article.)

The additional capacity losses are originated from deactivation of certain parts of the cell where the cover layer is so dense that no lithium-ions can be exchanged between anode and cathode. Thus in some part of the electrode the active lithium cannot be discharged or charged as the ion conductivity between anode and cathode is reduced to zero. The internal resistance is less affected than expected from the area covered with a compact layer as the duration of the pulse tests is just 10 s. Thus there is enough amount of residual electrolyte within the pores to return still good performance with respect to short-term pulses. The measurements of half-cells of the harvested anodes and cathodes reveal no change in capacity. This is still true for anodes showing a dense passivating covering layer on their top, as this layer shows cracks due to the unrolling of the jelly roll and is therefore now permeable to lithium-ions. Raman- and X-ray diffraction (XRD) measurements show no structural changes. Thus there is no evidence that a direct degradation of active material occurs.

This is in good agreement with literature where the existence of inhomogeneously distributed covering layers for cyclic aged LiFePO$_4$|Graphite cells is already reported. The covering layer is reducing the cells' performance like the internal resistance [6]. Furthermore the loss of active material is barely reported by Refs. [6,7,17] while the loss of active lithium is denoted as the major aging mechanism.

While the aging at 1 C and 50% and 100% does not show any difference with respect to capacity loss, all three cells aged at 10% DOD exhibit a significantly faster capacity fade. All tests are performed symmetrically with respect to 50% SOC. Between 45 and 55% SOC (10% DOD) there are no transitions of pure phases and only a very slight potential difference according to characteristics of the graphite anode displayed in Fig. 3. The cathode exhibits nearly no potential difference in this SOC range either. Thus inhomogeneous lithium distributions are not compensated by different potentials within both electrodes. And according to Hahn et al. nearly no volume change occurs within the graphite active material in the SOC range of 30–60% [18]. This missing volume change in this SOC range might lead to an inhomogeneous electrolyte distribution due to missing volume expansion of the anode. Finally the aging of those cells might even occur while the check-up of the test cells is performed assuming a high inhomogeneous lithium distribution. The post-mortem analyses of these cells exhibit the evolution of a local thick and dense cover layer plated on the anode facing the separator (Fig. 7). As small dendrites are observed, it is most likely that the origin of this covering layer is passivated lithium plating. The covering layer is clearly delimited and is formed in coating direction. Therefore the coating quality might be a driver for the covering layer evolution, too.

However, the reason for the covering layer evolution cannot be given within this publication. For NMC|Graphite cells Käbitz et al. showed that shallow cycling (with a stronger voltage slope of NMC compared to LFP) does not lead to faster aging [1].

The internal resistance is only increasing for remaining capacities lower than 80–85% for severe aging conditions and lower than 70% for mild aging conditions. As the increase of the internal resistance is correlated to the existence of dense covering layer it is very likely that the internal resistance is increased to some extend because of clogging pores of the anode close to the separator. The passivation of the lithium plating may as well dry out the electrolyte which will additionally affect the internal resistance.
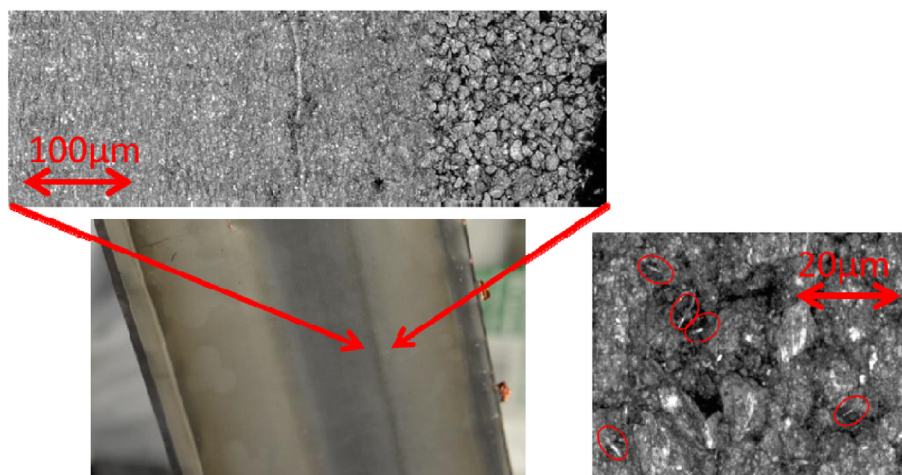

Fig. 7. Image of an anode (10% DOD 1 C) opened under argon atmosphere. The dark part is covered by a thick layer which can be observed by laser microscope imaging (confocal microscopy). At positions on the surface where the cover layer is less pronounced needle-like structures are found indicating lithium plating.

4. Conclusions

A test matrix of 50 cylindrical 8 Ah LiFePO$_4$|Graphite cells has been evaluated. The extrapolated calendaric lifetime down to 80% remaining capacity is over 20 years storing at 25 °C and over 3–4 years storing at 40 °C. Cycle lifetimes up to 2000–4800 FCE with current rates up to 4 C between 25 and 75% SOC can be achieved. Beside these good aging characteristics that would fulfill car manufacturers requirements the cells reveal a poor reproducibility in cycle tests, which manifests in extraordinary behavior of some cells. However, this drawback will help to understand certain processes within the cell that will be discussed elsewhere.

Furthermore it was shown that the geometric excess anode is influencing the initial trend of the capacity loss. Therefore the potential difference of the SOC before testing and the SOC during the tests according to the anode's potential are crucial to lithium-ion flow within the anode. The key driver for this effect is the potential difference between active and passive anode. On the basis of a simple approach the capacity increase could be explained. This initial capacity increase is superposed by the capacity fade due to calendaric aging. The aging up to 40 °C follows a linear-like trend and is featured by a high reproducibility. At 60 °C the aging becomes non-linear, the internal resistance is rising and the reproducibility of the cells' aging is very low. The influence of SOC on aging is quite low compared to the influence of temperature.

The given theory about the passive anode (Passive Electrode Effect) enables scientists to potentially understand certain peculiarities like the increase of capacity during aging over 100% of the initial capacity. The effect needs to be considered in measurements of self-discharge as the capacity loss of the cell according to the passive electrode effect is reversible as well and in the same order of magnitude as self-discharge. Furthermore capacity increases after longer interruption of testing or reversible capacity effects after changing the storage SOC can be explained in numerous cases by this theory. Thus the question needs to be raised at which SOC industrial cells should be typically delivered, as cells with a comparable nominal capacity that are delivered at 0% SOC and 100% SOC will have strongly different initial capacity losses during the first cycles. Thus datasheets should state the share of passive anode and the delivering SOC to provide the customer with a good technical base to compare industrial cells. Still it has an impact on the assumption that calendaric aging is following a $\sqrt{t}$ function as the initial trend due to the positive electrode effect is not included yet. Future simulations of lithium-ion batteries should comprise this theory as well, as the lateral flow of active lithium is in the first instance a reversible effect and can be separated from the actual aging that occurs in the cell. Therefore, the velocity of lateral flow of active lithium, according to potential differences and concentration differences, needs to be quantified in future work.

The cycle life tests point out that the cells may achieve lifetimes up to 2000–4800 FCE for C-rates of 1–4 C cycled between 25 and 75% SOC. A few cells behave anomalously and reveal several linear capacity loss phases that are followed by each other. More non-destructive tests and post-mortem analyses will be needed to understand the different disjunct and successively occurring aging phenomena. Astonishingly aging at 1C between 45 and 55% SOC is featured by stronger aging than 100% and 50% DOD. This effect is not yet well understood. The internal resistance of the high power cells is mostly constant or decreasing and is only rising rapidly if the remaining capacity becomes very low, if the tests are performed at 8 C or if cut-off voltages are reached during cycling.

The share of calendaric aging in cyclic aging was estimated to be 10–30% for nearly all tests. Thus the cycle life tests are not dominated by calendar lifetime.

References

[1] M. Ecker, N. Nieto, S. Käbitz, J. Schmalstieg, H. Blanke, A. Warnecke, D.U. Sauer, Calendar and cycle life study of Li(NiMnCo)O2-based 18650 lithium-ion batteries, J. Power Sources 248 (2014) 839–851, http://dx.doi.org/10.1016/j.jpowsour.2013.09.143.

[2] S. Käbitz, J.B. Gerschler, M. Ecker, Y. Yurdagel, B. Emmermacher, D. André, T. Mitsch, D.U. Sauer, Cycle and calendar life study of a graphite|LiNi1/3Mn 1/3Co1/3O2 Li-ion high energy system. Part A: full cell characterization, J. Power Sources 239 (2013) 572–583, http://dx.doi.org/10.1016/j.jpowsour.2013.03.045.

[3] J. Wang, P. Liu, J. Hicks-Garner, E. Sherman, S. Soukiazian, M. Verbrugge, H. Tataria, J. Musser, P. Finamore, Cycle-life model for graphite-LiFePO4 cells, J. Power Sources 196 (2011) 3942–3948, http://dx.doi.org/10.1016/j.jpowsour.2010.11.134.

[4] Y. Zhang, C.Y. Wang, X. Tang, Cycling degradation of an automotive LiFePO4 lithium-ion battery, J. Power Sources 196 (2011) 1513–1520, http://dx.doi.org/10.1016/j.jpowsour.2010.08.070.

[5] J. Purewal, J. Wang, J. Graetz, S. Soukiazian, H. Tataria, M.W. Verbrugge, Degradation of lithium ion batteries employing graphite negatives and nickel-cobalt-manganese oxide + spinel manganese oxide positives: Part 2, chemical-mechanical degradation model, J. Power Sources 272 (2014) 1154–1161, http://dx.doi.org/10.1016/j.jpowsour.2014.07.028.

[6] M. Klett, R. Eriksson, J. Groot, P. Svens, K. Ciosek Högström, R.W. Lindström, H. Berg, T. Gustafson, G. Lindbergh, K. Edström, Non-uniform aging of cycled commercial LiFePO4//graphite cylindrical cells revealed by post-mortem analysis, J. Power Sources 257 (2014) 126–137, http://dx.doi.org/10.1016/j.jpowsour.2014.01.105.

[7] M. Kassem, C. Delacourt, Postmortem analysis of calendar-aged graphite/LiFePO4 cells, J. Power Sources 235 (2013) 159–171, http://dx.doi.org/10.1016/j.jpowsour.2013.01.147.

[8] M. Reichert, D. Andre, A. Rösmann, P. Janssen, H.G. Bremes, D.U. Sauer, S. Passerini, M. Winter, Influence of relaxation time on the lifetime of commercial lithium-ion cells, J. Power Sources 239 (2013) 45–53, http://dx.doi.org/10.1016/j.jpowsour.2013.03.053.

[9] B. Gyenes, D.A. Stevens, V.L. Chevrier, J.R. Dahn, Understanding anomalous behavior in coulombic efficiency measurements on Li-Ion batteries, J. Electrochem. Soc. 162 (2015) 278–283, http://dx.doi.org/10.1149/2.0191503jes.

[10] A. Marongiu, F.G.W. Nußbaum, W. Waag, M. Garmendia, D.U. Sauer, Comprehensive study of the influence of aging on the hysteresis behavior of a lithium iron phosphate cathode-based lithium ion battery - an experimental investigation of the hysteresis, Appl. Energy 171 (2016) 629–645, http://dx.doi.org/10.1016/j.apenergy.2016.02.086.

[11] J. Belt, V. Utgikar, I. Bloom, Calendar and PHEV cycle life aging of high-energy, lithium-ion cells containing blended spinel and layered-oxide cathodes, J. Power Sources 196 (2011) 10213–10221, http://dx.doi.org/10.1016/j.jpowsour.2011.08.067.

[12] H.J. Ploehn, P. Ramadass, R.E. White, Solvent diffusion model for aging of lithium-ion battery cells, J. Electrochem. Soc. 151 (2004) A456, http://dx.doi.org/10.1149/1.1644601.

[13] M. Broussely, S. Herreyre, P. Biensan, P. Kasztejna, K. Nechev, R.J. Staniewicz, Aging mechanism in Li ion cells and calendar life predictions, J. Power Sources 97–98 (2001) 13–21, http://dx.doi.org/10.1016/S0378-7753(01)00722-4.

[14] S.F. Lux, I.T. Lucas, E. Pollak, S. Passerini, M. Winter, R. Kostecki, The mechanism of HF formation in LiPF6 based organic carbonate electrolytes, Electrochem. Commun. 14 (2012) 47–50, http://dx.doi.org/10.1016/j.elecom.2011.10.026.

[15] M. Dubarry, B.Y. Liaw, Identify capacity fading mechanism in a commercial LiFePO4 cell, J. Power Sources 194 (2009) 541–549, http://dx.doi.org/10.1016/j.jpowsour.2009.05.036.

[16] M. Lewerenz, J. Münnix, J. Schmalstieg, S. Käbitz, M. Knips, A. Warnecke, D.U. Sauer, New method evaluating currents keeping the voltage constant for fast and high resolved measurement of Arrhenius relation and capacity fade, J. Power Sources UNDER Rev. (2017). POWER-D-16–06222.

[17] M. Dubarry, C. Truchot, B.Y. Liaw, Cell degradation in commercial LiFePO4 cells with high-power and high-energy designs, J. Power Sources 258 (2014) 408–419, http://dx.doi.org/10.1016/j.jpowsour.2014.02.052.

[18] M. Hahn, H. Buqa, P.W. Ruch, D. Goers, M.E. Spahr, J. Ufheil, P. Novák, R. Kötz, A dilatometric study of lithium intercalation into powder-type graphite electrodes, Electrochem. Solid-State Lett. 11 (2008) A151, http://dx.doi.org/10.1149/1.2940573.